Journal of Magnetism and Magnetic Materials 460 (2018) 438–447

Contents lists available at ScienceDirect

Journal of Magnetism and Magnetic Materials

journal homepage: www.elsevier.com/locate/jmmm

Research articles

Exchange and magnetic order in bulk and nanostructured Fe_5Si_3

R. Skomski [a], P. Kumar [b,d], B. Balamurugan [a], B. Das [a], P. Manchanda [c], P. Raghani [d], A. Kashyap [e], D.J. Sellmyer [a,*]

[a] Department of Physics & Astronomy and Nebraska Center for Materials and Nanoscience, University of Nebraska, Lincoln, NE 68588, United States
[b] Department of Physics, University of Nebraska, Omaha, NE 68182, United States
[c] Department of Physics and Astronomy, Vanderbilt University, Nashville, TN 37235, United States
[d] Department of Physics, Boise State University, 1910 University Dr., Boise, ID 83725, United States
[e] School of Basic Sciences, IIT Mandi, Mandi, Himachal Pradesh, India

ARTICLE INFO

Article history:
Received 24 November 2017
Received in revised form 2 February 2018
Accepted 6 February 2018
Available online 31 March 2018

Keywords:
Curie temperature
Heisenberg model
Quantum spin liquids
Weak ferromagnetism

ABSTRACT

The Curie temperature of bulk and nanostructured Fe_5Si_3 is investigated using experiments, density-functional simulations, and many-body model calculations. The bulk intermetallic, which crystallizes in the hexagonal $D8_8$ structure, exhibits several intriguing features: it does not exist as a room-temperature equilibrium phase, is close to the onset of ferromagnetism, and exhibits two crystallographically very different Fe sites. The samples, produced by rapid quenching (bulk) and cluster deposition (nanoparticulate thin films), have Curie temperatures of about 400 K. Interatomic exchange constants are calculated using the Kohn-Korringa-Rostoker (KKR) method and used to solve the multisublattice mean-field problem for the system. The Vienna *ab initio* simulation package (VASP) is employed to study the dependence of the Fe moment on the thermally induced spin misalignment, and a model calculation yields an estimate for quantum-spin-liquid corrections. The theory includes Heisenberg exchange but overestimates the Curie temperature, and a discussion is given regarding additional approaches to handle weakly ferromagnetic multisublattice intermetallic compounds.

1. Introduction

The Curie temperature is one of the most important quantities in magnetism but surprisingly poorly understood, especially in structures with many non-equivalent sites, for example intermetallic alloys with big unit cells and magnetic nanostructures. Much of our understanding of finite-temperature magnetism is based on the Heisenberg model, where atomic spins $\mathbf{S}_i$ rotate due to thermal excitations [1–3]. However, the Heisenberg model, as well as other statistical models, such as the Ising model, imply strong electron-electron interactions (correlations), whereas electrons in itinerant 3*d* magnets are only weakly correlated. In the opposite limit, wave functions of electrons in periodic crystal potentials are of the Bloch type, characterized by well-defined wave vectors $\boldsymbol{k}$, and Bloch's simplified free-electron approach is the earliest model of itinerant magnetism [4]. It can be shown that the use of Bloch wave functions greatly overestimates the Curie temperature [5–10] and that the Heisenberg model is the qualitatively better starting point even for weakly correlated itinerant magnets.

Our focus is on bulk magnets and nanoparticle thin films of the weakly correlated intermetallic Fe_5Si_3. Iron-silicon alloys are among the best investigated and most widely used materials in modern technology. The production of soft-magnetic iron silicon for energy production and distribution exceeds that of any other magnetic material and accounts for about 40% of the combined production of all hard and soft magnets, especially in soft magnets for transformer cores [14]. Some other present or future applications include hydrogen production and spin electronics, the latter facilitated by the fact that iron-series transition-metal—silicon alloys tend to integrate well into electronic devices. Examples are Co_2Si gates in graphene electronics [15] and nanogranular Fe_5Si_3 in magnetoresistive devices [16]. Nanoparticles of Fe_5Si_3 have also attracted interest for medical applications, such as hyperthermia and drug administration [17].

Fe_5Si_3 has several intriguing physical properties. First, the hexagonal $D8_8$ structure of Fe_5Si_3 (Fig. 1) supports uniaxial magnetocrystalline anisotropy. While not desired in soft magnets, and uncommon in the iron-silicon system, this anisotropy is beneficial for some applications. Second, a characteristic but undesired

* Corresponding author.
E-mail address: dsellmyer1@unl.edu (D.J. Sellmyer).

https://doi.org/10.1016/j.jmmm.2018.02.015
0304-8853/

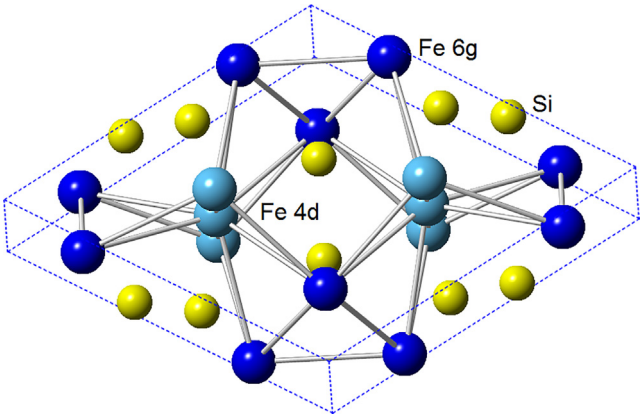

Fig. 1. Bulk crystal structure of Fe_5Si_3. The unit cell of the hexagonal bulk alloy contains 16 atoms, and the Fe occupies two nonequivalent sites, 4d (bright blue) and 6 g (dark blue). The 4d atoms form chains with small interatomic distances and large interatomic hopping. (For interpretation of the references to colour in this figure legend, the reader is referred to the web version of this article.)

feature is that the Si strongly suppresses magnetization and Curie temperature, about 380 K in bulk Fe_5Si_3 [18], with a sharp drop near the Fe_5Si_3 composition. Third, Fe_5Si_3 does not exist as a room-temperature equilibrium phase [19] but must be produced by nonequilibrium processing. Among the Fe_5Si_3 nanostructures fabricated so far are thin films [20], carbon-encapsulated nanoparticles [21], and nanowires having diameters in the range of 100–200 nm [22]. Fourth, $D8_8$-ordered Fe_5Si_3 exhibits two nonequivalent Fe sites (4d and 6g) with very different atomic environments.

Drops in Curie temperature are not uncommon in alloys of iron-series transition metals and metalloids. They reflect a dilution of the magnetism (reduced number z of transition-metal nearest neighbors) as well changes in the underlying quantum mechanics, typically a transition from strong to weak ferromagnetism. Strong ferromagnets, such as Co, are defined by completely filled minority bands, whereas weak ferromagnets, such as Fe, have partially empty minority bands (see e.g. the Appendices A and B). A good example of such a transition is Co_2Si [23], which is close to the transition between very weak itinerant ferromagnetism (VWIF) and exchange-enhanced Pauli paramagnetism in the bulk but becomes a strong ferromagnet in nanoparticle form. VWIF behavior is almost Stoner like [5–8,24,25] and far away from Heisenberg behavior.

Two very different mechanisms evolve as the temperature increases. First, on an independent-electron level, thermal spin disorder breaks the periodicity of the crystal. This effect, which is similar to the Anderson localization of electrons in aperiodic crystals [12], can be treated by density-functional theory (DFT) using the local spin-density approximation (LSDA) [11]. Second, electron-electron interactions (electron correlations) play a role at elevated temperatures, even in magnets that are well-described on an independent-electron level at zero temperature [10]. The localization equivalent of electron-electron interaction is Mott localization and the corresponding metal-insulator transition [13].

Correlations, as assumed in the Heisenberg model [3,26] and dominant in strongly correlated solids, reflect the Coulomb integral $\mathcal{U}$, that is, the energy necessary to accommodate an extra electron on an atom. The Coulomb integral competes against the one-electron energies parameterized by the interatomic hopping $\mathcal{T}$. Model calculations of interatomic exchange [3,26,27] yield a net exchange $\mathcal{J} = \mathcal{U} - \mathcal{T}$ in the weakly correlated limit $\mathcal{U} \ll \mathcal{J}$. In other words, ferromagnetic (FM) spin alignment ($\uparrow\uparrow$), which corresponds to $\mathcal{J} > 0$, is predicted for small band widths $W \sim \mathcal{T}$. Moment formation in narrow bands is indeed observed experimentally, but the corresponding Stoner-like criterion $\mathcal{U} \geqslant \mathcal{T}$ violates the original assumption of a small $\mathcal{U}$. Moreover, comparison of the $\uparrow\uparrow$ and $\uparrow\downarrow$ energies leads to the unphysical prediction of antiparallel (AFM) net exchange over the *entire range* of $\mathcal{U}/\mathcal{T}$, even in the Heisenberg limit of strong correlations, where $\mathcal{J} = -2\mathcal{T}^2/\mathcal{U}$. The resolution of this paradox require a careful distinction between inter- and intra-atomic exchange, but this distinction is not made by the Stoner theory and related independent-electron approaches. Overall, the treatment of correlations has remained a demanding challenge for decades, sophisticated methods being developed [10,31–33]. The main problem is that the number of involved quantum-mechanical configurations or Slater determinants increases exponentially with system size. For example, the complete description of a single CH_4 molecule (10 electrons and 2×8 basis functions) amounts to the diagonalization of a matrix containing 43758×43758 Slater determinants [10].

In contrast to correlations, aperiodic crystals are well described by independent-electron approaches. Kohn and Yaniv [34] have shown that the physical properties of such systems are determined on a local scale, even if the wave functions extend to infinity. They defined and calculated a local partition function (LPF) that yields the local density of states (LDOS). The LPF calculation can be performed separately for each nonequivalent atom in a structure, so that the total calculation time is linear in the number $\mathcal{N}$ of crystallographically nonequivalent sites, or $\mathcal{O}(\mathcal{N})$, as opposed to the $\mathcal{O}(\mathcal{N}^3)$ character of LSDA calculations. The range of the local environment that needs to be considered increases with the desired energy resolution. On a tight-binding level, the method reduces to the moments theorem [9,35]. Similar approaches exist for other properties. Wang, Wu, and Freeman [36] have shown that the magnetocrystalline anisotropy of transition-metal atoms can be approximated by a cluster (diatomic pair) model [36], and as in the Kohn approach, the accuracy of the method depends on the size of the cluster considered [37]. Of particular importance for the Curie temperature, and discussed in some detail in this paper, is the use of independent-electron first-principle calculations to determine interatomic Heisenberg exchange constants $\mathcal{J}_{ij}$ for itinerant magnets [11]. The $\mathcal{J}_{ij}$ form an $\mathcal{N} \times \mathcal{N}$ matrix that must be diagonalized to yield the Curie temperature as the largest eigenvalue of the matrix [27,38].

In this paper, we investigate Fe_5Si_3 magnets experimentally and theoretically, using independent-electron first-principle simulations and many-electron model calculations. The aim of this paper is not to improve or sophisticate existing DFT [39–41,82] and correlation [42–45] treatments, but to analyze how different physical mechanisms affect the Curie temperature. Furthermore, no attempt is made to accurately reproduce the Curie temperature through parameter and method refinement, which is *de facto* a second-principle approach. We investigate the Curie temperature as a function of Si content and real structure (Section 2), present first-principle calculations of the interatomic exchange (Section 3), and use model calculations to explore quantum-liquid corrections to the Curie temperature (Section 4).

2. Experiment

The Fe-Si phase diagram contains several Fe-rich phases, but some of them form at high temperatures only, above 825 °C in the case of Fe_5Si_3 [19]. To produce this phase, it is necessary to use non-equilibrium synthesis methods. The samples, namely single-phase Fe_5Si_3 nanoparticles, have been produced by gas-aggregation cluster deposition [47] and bulk Fe_5Si_3 prepared by arc-melting and subsequent melt-spinning.

Fe_5Si_3 crystallizes in the hexagonal $D8_8$ structure (prototype Mn_5Si_3), characterized by the point group D_{6h} and the space group

$P6_3/mcm$. Fig. 1 shows a unit cell of Fe_5Si_3, which contains two formula units (16 atoms). The Fe atoms occupy two different crystallographic sites, namely 4d sites (bright blue) with the coordinates (1/3, 2/3, 0), (2/3, 1/3, 0), (1/3, 2/3, 1/2), and (1/3, 1/3, 1/2), and 6 g sites (dark blue) with the coordinates (x, 0, 1/4), (0, x, 1/4), (1–x, 1–x, 1/4), (1–x, 0, 3/4), (0, 1–x, 3/4), and (x, x, 3/4), where $x = 0.24$. The Si atoms also occupy Wyckhoff 6 g positions but have $x = 0.606$. The lattice constants of bulk Fe_5Si_3 are $a = b = 6.722$ Å and $c = 4.680$ Å. The 4d atoms form chains with small interatomic distances, which is important for the understanding of the material.

Fig. 2 shows the Curie temperature of bulk and nanoparticle Fe_5Si_3 for different stoichiometries close to the ideal 5:3 composition (37.5 at.% Si), varied by adjusting the target composition. The nanoparticle Curie temperature is somewhat higher than the bulk T_c and comparable to those obtained for other nanostructures [17,22] of Fe_5Si_3. In a strict sense, the Curie temperature of zero-dimensional magnets (nanoparticles and clusters) is zero, because the partition function $\mathcal{Z} = \Sigma_\mu \exp(-\mathscr{H}_\mu/k_BT)$ of any finite system is free of singularities [25,46]. Nanoparticle experiments actually probe intraparticle spin-spin correlations, whose decay is reminiscent of the bulk $M(T)$ behavior with finite-size corrections, meaning that T_c somewhat decreases with particle size [25]. Furthermore, the present Curie temperatures were measured on Si (0 0 1) substrates densely covered with nanoparticles, so that the T_c is actually that of a nanoparticulate magnet.

Bulk Fe_5Si_3 is a weak ferromagnet with a substantial number of holes in the majority band, similar to bcc Fe, whereas the surface is strongly ferromagnetic with virtually no holes in the majority band (Appendix A). This situation is similar to that encountered in Mn_5Si_3 nanoparticles [47]. The bulk behavior is consistent with earlier Mössbauer data [18], which indicate that the Fe on the 4d sites is not fully spin-polarized.

3. Site-Specific Curie-Temperature analysis

The Heisenberg analysis of alloys such as Fe_5Si_3 requires the consideration of two or more elements on several transition-metal sublattices. The mean-field behavior of multisublattice magnets is well-understood and was first investigated for ferrimagnetic oxides, such as magnetite (Fe_3O_4) and yttrium garnet YFe_5O_{12} [38,48,49]. Each of the $\mathcal{N}$ nonequivalent sites experiences an individual mean field, and the Curie temperature corresponds to the largest eigenvalue of the corresponding $\mathcal{N} \times \mathcal{N}$ matrix $\mathcal{J}_{ij}$. In this section, it is convenient to define the Heisenberg model using normalized spin vectors,

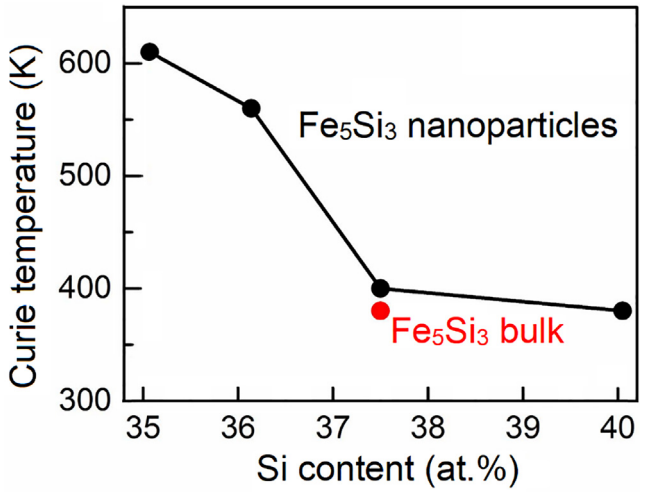

Fig. 2. Curie temperature of Fe_5Si_3 as a function of Si content.

$$\mathcal{H} = -\Sigma_{i>j}\, \mathcal{J}_{ij} \frac{\mathbf{S}_i \cdot \mathbf{S}_j}{S_i S_j} - 2\, \mu_B\, \mu_o\, \Sigma_i\, \boldsymbol{H}_i \cdot \mathbf{S}_i \qquad (1)$$

where $\mathcal{J}_{ij}$ is the exchange energy *per bond* and $\boldsymbol{H}_i$ is the magnetic field acting on the i-th atom. The factor $1/S_iS_j$ ensures a meaningful normalization $\mathbf{S}^2/S^2 = S(S+1)/S^2 = 1$ in the classical limit ($S = \infty$). Applying the statistical mean-field approximation to Eq. (1) yields

$$T_c = \frac{S+1}{3Sk_B}\, \mathcal{J}_{\text{eff}} \qquad (2)$$

This expression is widely used for Fe and Co atoms, using the approximations $S = 1$ and $\mathcal{J}_{\text{eff}} = \Sigma_j \mathcal{J}_{0j}$, where the summation contains all neighbors of atom 0. Considering nearest neighbors only ($\mathcal{J}_{ij} = \mathcal{J}$) yields $\mathcal{J}_{\text{eff}} \approx z\mathcal{J}$, where z is the number of nearest neighbors. When a solid is very inhomogeneous, then the Curie temperature is largely determined by the sublattices with the strongest exchange coupling [50]. In this case, averaging over all $\mathcal{J}_{0j}$ does not work and the $\mathcal{J}_{ij}$ must be calculated and evaluated explicitly.

We have also performed spin-polarized relativistic Kohn-Korringa-Rostocker (SPR-KKR) Green-function calculations [51–53] to determine the exchange interactions $\mathcal{J}_{ij}$ in bulk and thin-film Fe_5Si_3. The calculation determines spin-spin interaction energies $E_{ij} = -\mathcal{J}_{ij} \cos\theta_{ij} \approx -\mathcal{J}_{ij} + \frac{1}{2}\, \mathcal{J}_{ij}\, \theta_{ij}^2$, where θ_{ij} is the angle between atomic spins i and j. The calculation is of the independent-electron type and evaluates multiple electron scattering during which the spin misalignment θ_{ij} is treated as a small perturbation.

Since atoms on the same sublattice have the same magnetization, it is sufficient to consider $\mathcal{J}_{ab}$, where a and b are sublattice indices and each $\mathcal{J}_{ab}$ is a sum over many neighbors in sublattice b. The sum includes all b atoms in the unit cell where an a-atom is located but also b atoms in neighboring unit cells, depending on the desired accuracy. Since Fe_5Si_3, contains two nonequivalent sites (4d and 6h), $\mathcal{J}_{ab}$ is a 2×2 matrix. In more detail, the underlying linearized mean-field field equations for the two Fe sublattices are

$$T_c\langle m_{4d}\rangle = \frac{S+1}{3Sk_B}\left(\langle m_{4d}\rangle \Sigma_i \mathcal{J}_{4d,i} + \langle m_{6g}\rangle \Sigma_j \mathcal{J}_{4d,j}\right) \qquad (3a)$$

$$T_c\langle m_{6g}\rangle = \frac{S+1}{3Sk_B}\left(\langle m_{4d}\rangle \Sigma_i \mathcal{J}_{6g,i} + \langle m_{6g}\rangle \Sigma_j \mathcal{J}_{6g,j}\right) \qquad (3b)$$

where $S \approx 1$ is the Fe spin and the i and j summations refer to 4d and 6h sites, respectively. Up to an interatomic distance of $R = 4.1$ Å, there are 19 Fe-Fe bonds, all listed in Table 1.

Note that the procedure leading to Eq. (3) cannot be applied to 'nonmagnetic' elements, such as Si in Fe_5Si_3. The nearest and next-nearest neighbors of the Fe 6g atoms in bulk Fe_5Si_3, are Si, and the KKR Fe-Si calculations yield $\mathcal{J}_{ij}$ values of 1.164 and 0.87 meV, respectively. However, the small Si moments, which are of the order of 0.1 μ_B, are induced by Fe neighbors, which have moments m_{Fe} of about 1.5 μ_B per atom. Since the individual Si moments are determined by the surrounding Fe spins, they cannot be treated as degrees of freedom and must be excluded from the summation in the partition function. This explains the absence of Si terms in Eq. (3), a point that will be further discussed below.

Performing the i and j summations in Eq. (3) yields

$$T_c\langle m_{4d}\rangle = \frac{S+1}{3Sk_B}\left((2\mathcal{J}_1 + 3\mathcal{J}_2)\langle m_{4d}\rangle + 6J^*\langle m_{6g}\rangle\right) \qquad (4a)$$

$$T_c\langle m_{6g}\rangle = \frac{S+1}{3Sk_B}\left((4\mathcal{J}^*\langle m_{4d}\rangle + 2)(\mathcal{J}' + \mathcal{J}'')\langle m_{6g}\rangle\right) \qquad (4b)$$

The solution of this set of equation amounts to the diagonalization of the matrix

Table 1
Iron-iron exchange bonds in bulk Fe_5Si_3.

$\mathcal{J}_{ij}$	Sublattices	R (Å)	Z	$\mathcal{J}_{ij}$ (meV)
$\mathcal{J}_1$	4d–4d	2.34	2	42.34
$\mathcal{J}'$	6g–6g	2.80	2	18.09
$\mathcal{J}''$	6g–6g	2.84	2	14.08
$\mathcal{J}^*$	4d–6g	2.86	6	11.85
$\mathcal{J}^*$	6g–4d	2.86	4	11.85
$\mathcal{J}_2$	4d–4d	3.88	3	6.94

$$\begin{pmatrix} 2\mathcal{J}_1+3\mathcal{J}_2 & 6\mathcal{J}^* \\ 4\mathcal{J}^* & 2(\mathcal{J}'+\mathcal{J}'') \end{pmatrix} = \begin{pmatrix} 105.5 & 71.1 \\ 47.4 & 64.3 \end{pmatrix} \text{meV} \tag{5}$$

The Curie temperature is given the largest eigenvalue $\mathcal{J}^+$ of this interaction matrix, namely

$$\mathcal{J}^+ = \mathcal{J}_1 + 3\mathcal{J}_2/2 + \mathcal{J}' + \mathcal{J}'' + \sqrt{(\mathcal{J}_1 + 3\mathcal{J}_2/2 - \mathcal{J}' - \mathcal{J}'')^2 + 24\mathcal{J}^{*2}} \tag{6}$$

Explicitly, $\mathcal{J}^+$ = 146.5 meV. The Curie-temperature value corresponding to $\mathcal{J}_+$ is 1133 K, higher than the experimental value. The reasons for this disagreement will be discussed in Sections 4 and 5.

To study nanoscale surface effects [54], we have also considered a (0 0 1) oriented thin film of Fe_5Si_3. Fig. 3 shows the corresponding supercell. The relationship between the supercell and the bulk unit cell of Fig. 1 is visible most easily by looking at the 4d Fe atoms (light blue), which form chains along the z-direction in both figures. There are 5 rather than 2 nonequivalent Fe sublattices, distinguishing Fe atoms with different vertical positions. The bulk Fe 6 g sublattice (dark blue) splits into two sublattices, depending on whether the atoms are near the surface or in the interior of the film. The 4d sublattice (light blue) splits into 3 sublattices, depending on whether the atoms are located at the surface, below the surface, or in the central plane of the film.

The mean-field description of the system of Fig. 3 requires the first-principle calculation of hundreds of $\mathcal{J}_{ij}$ but, similar to the transition from Eqs. (3) and (4), the individual atomic interactions can be collected in form of inter- and intrasublattice exchange constants. The corresponding 5 × 5 matrix is

$$\mathcal{J}_{ab} = \begin{pmatrix} -5.1 & 18.7 & 50.7 & -1.7 & -3.7 \\ 12.5 & 55.5 & 30.8 & 29.0 & 1.0 \\ 50.7 & 46.1 & -13.3 & 18.8 & 32.4 \\ -1.1 & 29.0 & 12.6 & 52.8 & 12.2 \\ -7.4 & 2.9 & 64.6 & 36.5 & -12.8 \end{pmatrix} \text{meV} \tag{7}$$

The largest exchange, 55.5 meV, is the intrasublattice exchange between the dark blue atoms near the surface. Surprisingly, however, the largest eigenvalue of Eq. (7), $\mathcal{J}^+$ = 114.4 meV, is smaller than the bulk value $\mathcal{J}^+$ = 145.5 meV. The net reduction of the predicted T_c contradicts the experimental result of Fig. 2 and means that the increased exchange near the surface is not able to overcompensate the reduced number z of Fe neighbors near the surface.

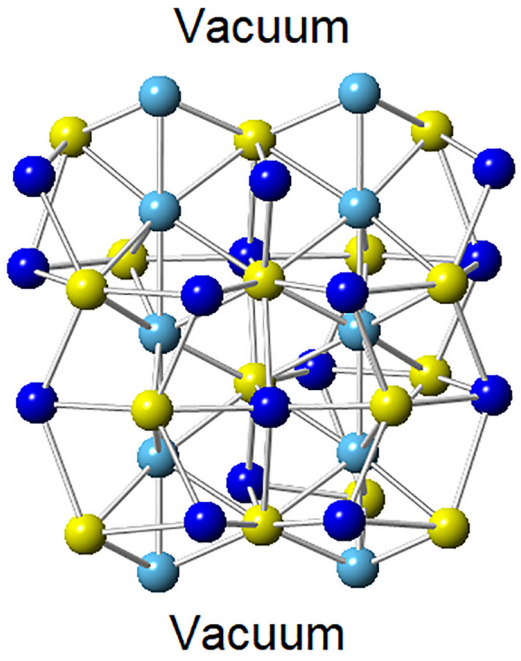

Fig. 3. Fe_5Si_3 supercell used in the thin-film calculations.

4. Heisenberg interactions in itinerant magnets

The mean-field approximation behind Eqs. (7) is well-known to overestimate the Curie temperature, because it ignores critical fluctuations [55,56]. Experiment, model calculations, and Monte-Carlo simulations shows that critical fluctuations reduce T_c by a factor of order two [55–57]. To a large extent, this accounts for the high absolute values of T_c (more than 1000 K), but it does not explain why the calculated thin-film Curie-temperature is smaller than the bulk one. The effect of critical fluctuations increases with decreasing dimensionality, so the inclusion of critical fluctuations would further reduce the thin-film T_c relative to the bulk T_c, in contradiction to experiment.

Our explanation, to be elaborated below, is that bulk Fe_5Si_3 is fairly close to the onset of ferromagnetism, or to a transition between weak and strong ferromagnetism. Fig. 2 is an experimental manifestation of transition, namely a strong Curie-temperature decrease in a very narrow concentration range. Heisenberg exchange is proportional to $\mathbf{S}_i \cdot \mathbf{S}_j$, so that the $\mathcal{J}_{ij}$ in Eq. (1) scale as $S^2 \sim m_{Fe}^2$, and near a quantum phase transition, minor changes in structure and computational methods may yield big changes in m_{Fe}. The present SPR-KKR calculations, which determine atomic magnetic moments as a part of the calculation, yield a moment of m = 1.76 μ_B, compared to 1.35 μ_B in our VASP calculations (Appendix A) and 1.27 μ_B in Ref. [61]. Judging from the experimental hyperfine fields of 130 kOe (4d) and 220 kOe (6h) [18], the experimental value is not much bigger than 1.2 μ_B. Such large variations do not occur in strong (Co) or nearly strong ferromagnets (bcc Fe) but are expected in very weak (VWIF) regime.

Aside from numerical accuracy, which lies beyond the scope of this paper, the Heisenberg description of Fe_5Si_3 gives rises to more fundamental questions of direct importance to the Curie-temperature problem. By definition, Heisenberg moments S are integer or halfinteger, and the ratio $(S+1)/S$ in Eq. (4) is quantum-mechanically ill-defined for intermediate values of S. In fact, the itinerant character of the Fe 3d electrons means that $m = 2S$ μ_B can assume arbitrary values, including near-zero moments in very weak itinerant ferromagnets. In Sections 4.1 and 4.2, respectively, we will outline how this question is tackled on an LSDA level and to what extent the LSDA can be improved. Section 4.1 is devoted to the problem that Heisenberg model strongly correlated model with spin-liquid-like features, as contrasted to the limit of weak correlations in itinerant ferromagnets.

4.1. The Heisenberg model and the independent-electron approximation

Density-functional calculations using the local-spin-density approximation (LSDA) are basically on an independent-electron level, using a single Slater determinant. The theory has been very successful in describing weakly correlated electrons in solids, and there are no indications that correlations are strong in Fe_5Si_3. To determine the density functional, L(S)DA uses a Schrödinger-like wave equation, namely the Kohn-Sham (KS) equation [58–60]. Fig. 4 shows the underlying physics, namely a single electron in a selfconsistently determined distribution of electrons described by spin-dependent densities $n(\mathbf{r})$ (gray). Due to its similarity with the statistical mean-field approximation, the approach is also referred to as quantum-mechanical mean-field approximation. This characterization includes the LSDA + U approximation (Appendix B).

Of course, the apparently simple picture of Fig. 4 does not mean that solving the LSDA problem is trivial. In a periodic solid, the crystal potential $V(\mathbf{r})$ yields a shell structure for each atom, including partially filled 3*d* shells in iron-series transition metals, and a generally very complicated band structure due to interatomic hybridization.

The LSDA is very powerful in determining the energy as a function of a crystal potential $V(\mathbf{r})$, and this includes spin-dependent potentials. In the simplest case, ↑ and ↓ electrons experience different potentials, corresponding to ferro-, ferri-, or antiferromagnetism. The origin of the different ↑ and ↓ potentials is the Coulomb repulsion $\mathcal{U}$. The Pauli principle forbids pairs of ↑↑ and ↓↓ electrons in any given orbital and means that electrons of parallel spins stay away from each other. By contrast, ↑↓ and ↓↑ pairs are allowed by the Pauli principle but cost Coulomb energy, and this energy is responsible for the formation of the atomic moments.

The method can be used to describe arbitrary spin directions if the spin-dependent part

$$V_{\uparrow,\downarrow} = -U_o\begin{pmatrix}1 & 0\\ 0 & -1\end{pmatrix} \tag{8}$$

of the potential is replaced by

$$V_\sigma = -U_o\left(\begin{pmatrix}0 & 1\\ 1 & 0\end{pmatrix}\sigma_x + \begin{pmatrix}0 & -i\\ i & 0\end{pmatrix}\sigma_y + \begin{pmatrix}1 & 0\\ 0 & -1\end{pmatrix}\sigma_z\right) \tag{9}$$

Here σ is the unit vector of the local spin direction and $U_o \sim \mathcal{U}$ is a Stoner-like Coulomb parameter. Physically, the spin is allowed to rotate, as schematically shown in Fig. 4, and the spin angle may vary throughout the crystal. This approach can be used to treat arbitrary spin configurations $\sigma_i = \sigma(\boldsymbol{R}_i)$, including zero-temperature noncollinearity, caused for example by competing exchange [27], and thermal spin disorder [11,28–30]. In particular, the approach can be used to determine the interaction energies $\mathcal{J}_{ij}$ [11]. For example, to calculate the ferromagnetic energy, one takes $\sigma_i = \boldsymbol{e}_z$, an antiferromagnetic energy calculation requires $\sigma_i = \pm e_z$, depending on the crystal site, and at the Curie temperature, all directions of σ_i must be considered.

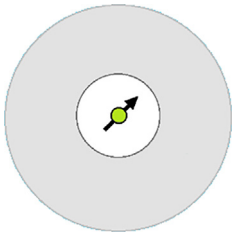

Fig. 4. Independent electron (center) in a selfconsistently treated sea of surrounding electrons (gray).

The method is, in principle, very accurate, but it is poorly adapted to the Heisenberg model which is subsequently used to determine the Curie temperature. By definition, the partition function $\mathcal{Z}$, which determines T_c, is a sum over the *eigenstates*, and fixing the configuration σ_i in a DFT calculation violates this criterion. Consider, for example, neighboring electrons 1 and 2 having their respective spins in the *z*-direction ($\theta = 0$) and rotated by a nonzero angle θ. Based on Eq. (9), the two spin wave functions are $\psi_1(0) = (1, 0)$ and $\psi_2(\theta) = (\cos\tfrac{1}{2}\theta, \sin\tfrac{1}{2}\theta)$. Using these wave functions to evaluate the Heisenberg Hamiltonian $\mathcal{H} = -\mathcal{J}\ \sigma_1\cdot\sigma_2$ for $\theta = \pi$ yields the respective ↑↓ and ↑↑ energies $\pm\mathcal{J}$. By contrast, the well-known *exact* eigenstates of the two-electron problem

$$\mathcal{H} = \mathcal{J}\begin{pmatrix}-1 & 0 & 0 & 0\\ 0 & 1 & 2 & 0\\ 0 & 2 & 1 & 0\\ 0 & 0 & 0 & -1\end{pmatrix} \tag{10}$$

are an FM triplet of energy $-\mathcal{J}$ and an AFM singlet of energy $+3\mathcal{J}$. In terms of Fig. 4, the AFM wave function

$$\Psi = \frac{1}{\sqrt{2}}\left(\uparrow\downarrow - \downarrow\uparrow\right) \tag{11}$$

As mentioned in the introduction, $\mathcal{J} = -2\mathcal{T}^2/\mathcal{U}$ is negative in the model, so that the AFM energy is reduced as compared to the FM energy, doubling the level spacing from $2\mathcal{J}$ to $4\mathcal{J}$.

It is worthwhile emphasizing that the doubling of the level spacing and of the corresponding Néel-like ordering temperature is a quantum effect. For arbitrary spins, the splitting can be shown to increase by a factor $1 + 2/S$. This means that Fe and Co ($S \approx 1$) carry an error of the order of 50%, whereas in the classical limit, $S = \infty$, the error is zero. In other words, Heisenberg exchange constants $\mathcal{J}_{ij}$ obtained through DFT calculations are generally very accurate but correspond to the classical Heisenberg model, characterized by continuous magnetization angles, which leads to overestimation of AFM energies and of T_c.

4.2. Quantum spin-liquid (QSL) corrections

In Section 4.1, we have shown how wave functions are important for the understanding of the Curie temperature. In weakly correlated systems, such as Fe_5Si_3, the problem is the Heisenberg interpretation of the $\mathcal{J}_{ij}$ rather than the $\mathcal{J}_{ij}$ values themselves. Density-functional theory deemphasises wave functions and ignores wave-function-specific features such as quantum entanglement between subsystems [83–87]. For example, the two-electron state $|a\rangle|b\rangle - |b\rangle|a\rangle$ is maximally entangled, as contrasted to the separable state $|a\rangle|b\rangle = |a\,b\rangle$. The entanglement behavior is different for FM and AFM configurations, which has far-reaching consequences for the ordering temperature.

A well-understood system is the AFM Heisenberg chain, whose ground state is a quantum spin liquid without long-range order but with slowly decaying spin correlations [3,88]. The ferromagnetic ground state is a single spin configuration, symbolically $|\Psi_{FM}\rangle = |\uparrow\uparrow\uparrow\uparrow\uparrow\uparrow\uparrow\uparrow\rangle$. Other spin configurations (or Slater determinants) are not allowed in the FM ground state, because the hopping of a ↑ electron onto a neighboring ↑ site is forbidden by the Pauli principle. A naïve expectation for the ground state is one of the Néel states

$$|\Psi_{AFM}(1)\rangle = |\uparrow\downarrow\uparrow\downarrow\uparrow\downarrow\uparrow\downarrow\rangle \tag{12a}$$

and

$$|\Psi_{AFM}(2)\rangle = |\uparrow\downarrow\uparrow\downarrow\uparrow\downarrow\uparrow\downarrow\rangle \tag{12b}$$

or a superposition of the two states. However, the Heisenberg Hamiltonian contains the product $\mathbf{s}_i \cdot \mathbf{s}_j$, which can be written as

$$\mathbf{s}_i \cdot \mathbf{s}_j = 1/2\left(s_i^+ s_j^- + s_i^- s_j^+\right) + s_i^z s_j^z \tag{13}$$

where $s^\pm = s_x \pm i s_y$. In Eq. (13), the s_z operators merely count the spins and leave the wave function unchanged, aside from a trivial factor ±1, whereas the $s^\pm$ terms interchange spins *i* and *j*. The Néel states cannot be eigenvectors of the Heisenberg Hamiltonian, because the spin-flip terms in Eq. (13) create pairs of parallel spins (spinons), for example $s_4^+ s_5^+ \ |\uparrow\downarrow\uparrow\downarrow\uparrow\downarrow\uparrow\downarrow\rangle = |\uparrow\downarrow\uparrow\uparrow\downarrow\downarrow\uparrow\downarrow\rangle$. The ground state of the AFM Heisenberg chain is therefore a liquid-like superposition of many spin-flip configurations, which can be treated for example with the help of the Bethe ansatz [89–91].

The Bethe ansatz and the corresponding quantum-spin-liquid behavior are limited to one dimension, but related corrections can be expected near quantum-phase transitions (QPT) [92], including the transition from exchange-enhanced Pauli paramagnetism to VWIF. Furthermore, reduced dimensionality (nanoparticles and thin films) is likely to enhance quantum fluctuations. We will not be able to quantitatively solve the problem in this section, but present a many-electron model that outlines the basic nature of the corrections.

Fig. 5 shows the corresponding cluster model. In contrast to Fig. 4, the environment of the central spin is no longer modeled as a quantum-mechanical mean field but individualized through *z* nearest neighbors. The interaction between the central spin and the surrounding spins is assumed to be of the $S = 1/2$ Heisenberg type, described by nearest-neighbor exchange $\mathcal{J}$.

To calculate the many-electron wave functions and energies, we exploit that the $S = 1/2$ Heisenberg model can be mapped onto a hardcore-boson model [90,91,93], as schematically outlined in Fig. 6. In the model, ↑ and ↓ correspond to filled and empty boxes, respectively, and the exchange integrals $\mathcal{J}_{ij}$ are analogous to a hopping integral $\mathcal{T}_{ij}$. The analogy allows an intuitive evaluation of the many-electron configuration-interaction (CI) matrix elements, without nontrivial quantum mechanics. First, the matrix elements are nonzero, essentially $\mathcal{J}$ or $\mathcal{T}$, only if one hard-core boson moves to an empty neighboring site. Second, the number of bosonic particles is conserved, so that the determination of the state closest to the FM state involves the switching of one spin only, or one unoccupied site in the bosonic model. This reduces the number of configurations to be considered from 2^{z+1} to $z+1$. Both the identification of the non-zero matrix elements and the particle number conservation are a consequence of the commutation behavior of Eq. (13). The ferromagnetic state of the model of Fig. 5 has the energy $-z\mathcal{J}$, each exchange bond contributing an energy of $-\mathcal{J}$. The energy of the state with one reversed spin is obtained by diagonalizing the $(z+1) \times (z+1)$ matrix

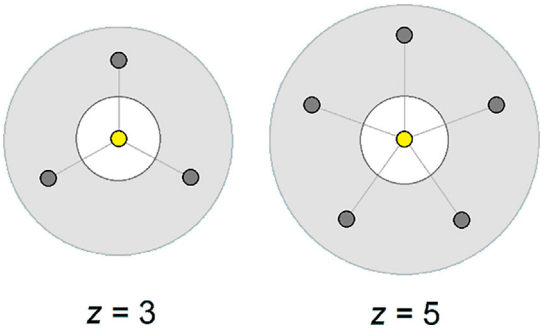

Fig. 5. Model describing quantum-spin-liquid corrections in solids. Assuming that the atomic spins are of the $S = 1/2$ Heisenberg type, there are 2^{z+1} spin configurations (Slater determinants), that is, for example 64 configurations in the case of $z = 5$.

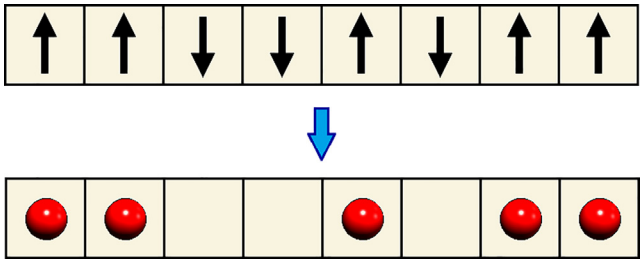

Fig. 6. Interpretation of the Heisenberg model as a hardcore-boson model.

$$\mathcal{H} = -\mathcal{J}\begin{pmatrix} z-2 & 0 & \dots & 0 & 0 & 2 \\ 0 & z-2 & \dots & 0 & 0 & 2 \\ \dots & \dots & \dots & \dots & \dots & \dots \\ 0 & 0 & \dots & z-2 & 0 & 2 \\ 0 & 0 & \dots & 0 & z-2 & 2 \\ 2 & 2 & \dots & 2 & 2 & z-2 \end{pmatrix} \tag{14}$$

This matrix means that the central spin can exchange-interact with all other spins (last column and row), whereas the peripheral spins interact with the central spin only. The diagonalization of Eq. (14) yields eigenfunctions $\Psi(z)$ where half the weight is localized at the central spin and the remainder equally distributed over the *z* peripheral spins. For example, in the case of $z = 3$,

$$\Psi = \frac{1}{\sqrt{2}} - \frac{1}{\sqrt{6}}\left(+ + \right) \tag{15}$$

This wave function illustrates the liquid-like character of configurations with AFM bonds: the reversed spin (yellow) is not confined to a single atom but 'leaks' into the crystalline environment.

Using the eigenfunctions $\Psi(z)$ yields the energy eigenvalues

$$E_\Psi = -\mathcal{J}(z - 2 - 2\sqrt{z}) \tag{16}$$

The square-root term in this equation describes quantum corrections going beyond the switching of the central spin. In terms of Eq. (15), they correspond to the three terms in the parentheses of Eq. (15). Normalized by the mean-field energy difference $2z\mathcal{J}$, the energy and Curie-temperature corrections vary between 71% for $z = 2$ (e.g. the 4d atoms in Fe_5Si_3) and 29% for $z = 12$ (e.g. fcc crystals). While the model is rather crude, it outlines the role of quantum fluctuations in magnetic ordering.

5. Discussion and conclusions

The analysis of the preceding sections indicates a dilemma. The partition functions behind the Curie-temperature determination in both model calculations and Monte-Carlo simulations are commonly based on the Heisenberg model, but the spin states considered in DFT calculations are weakly correlated and not eigenstates of the Heisenberg Hamiltonian. For example, the Heisenberg model assumes a rotation of spins of fixed magnitude $\mathbf{S}^2 = S(S+1)$, but itinerant ferromagnets exhibit noninteger atomic moments. In the case of Fe_5Si_3, the calculated local densities of states (Appendix A) indicate that the ferromagnetism of the Fe atoms near the particle surface is strong, characterized by a fully occupied majority 3*d* band, whereas that in the bulk is weak, with many holes in the majority band. Structurally, this weak itinerant feature is associated with the very small distance between neighboring iron atoms on the 4d sites of the hexagonal 5:3 structure. The quasi-classical character of the Heisenberg interpretation of itinerant magnetism yields a fairly substantial error.

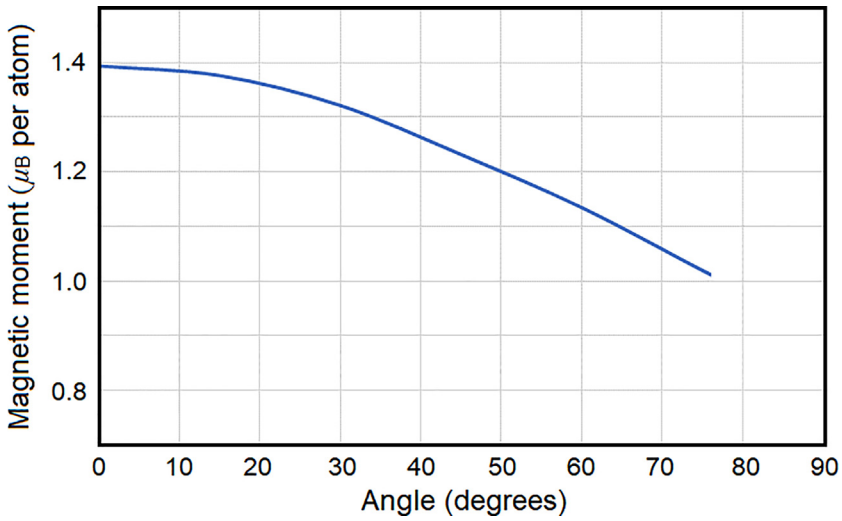

Fig. 7. Calculated magnetic moments of the Fe 4d atoms in bulk Fe_5Si_3 as a function of the angle between neighboring atomic spins. The spin misalignment is created by thermal excitations.

An important non-Heisenberg effect in itinerant magnets is that the magnitude $|\boldsymbol{m}|$ of the atomic moments may actually change during spin rotation, moments decreasing with increasing misalignment angle [10]. The weaker the ferromagnetism, the more pronounced the moment reduction [8,24], an extreme case being the completely collapse of the atomic moments if they are forced to form AFM sublattices. Since the Curie temperature scales as $S(S+1) \sim m^2$, the moment reduction is accompanied by a pronounced Curie-temperature reduction.

Fig. 7 shows the moment of the Fe 4d atoms (light blue in Fig. 1) in bulk Fe_5Si_3 as a function of the angle θ between 4d nearest neighbors, calculated using VASP. The calculation is numerically unstable near and above 80°, but fitting $m(\theta)$ to a parabolic curve and integrating m^2 over random spin angles θ yields Curie-temperature reduction by 30.7%. This reduction adds to reductions due to critical fluctuations and quantum fluctuations. Due to the reduced number of neighbors, the effect is much less pronounced at surfaces and nanoparticles whose magnetism is strong.

In conclusion, we have analyzed and semiquantitatively explained the Curie temperature of bulk and nanostructured Fe_5Si_3. The material is close to the onset of ferromagnetism, which makes the Curie temperature sensitive to a variety of corrections. Our KKR first-principle calculations overestimate the Curie temperature by a factor of about three. The neglect of critical thermodynamic fluctuations accounts yields an overestimation by a factor of about two, which is a well-known phenomenon and treatable by statistical methods such as Heisenberg Monte-Carlo simulations. Our model calculations indicate that spin-liquid-like Heisenberg quantum fluctuations yield difficult-to-quantify corrections of up to several 10%, generally reducing the Curie temperature. Finally, spin fluctuations in weak itinerant ferromagnets are poorly described by the Heisenberg model, because these magnets are weakly correlated, in contrast to the strongly correlated Heisenberg model. Our VASP calculations indicate that the corresponding corrections yield a further Curie-temperature reduction of up to 30% in the bulk but not at surfaces and in small particles. Our analysis shows that quantitatively accurate Curie temperature calculations for weak ferromagnets with multiple sublattices remain a practical challenge.

Acknowledgements

The primary support for this research is through DOE-BES (DE-FG02-04ER46152, R.S. and D.J.S), complemented by NSF-DMREF (SusChEM, Award Number 1436385, experiment, B.D. and B.B.), the Nebraska Center for Materials and Nanoscience, and the Holland Computing Center.

Appendix A. VASP density-functional calculations

Density functional theory (DFT) calculations are performed using projected augmented wave method (PAW) [94], as implemented in the Vienna *ab initio* simulation package (VASP) [95,96]. For the structural relaxation and the electronic-structure calculations, we have used a generalized-gradient approximation (GGA) with Perdew–Burke–Ernzerhof (PBE) exchange-correlation functional [39]. The electron wave functions are expanded in a plane-wave basis set with an energy cutoff of 500 eV and the calculations are performed using experimental lattice parameters. For the bulk calculations, a $9 \times 9 \times 11$ Monkhorst-Pack grid for k-point sampling is used [97]. In the nanocluster calculations, the Γ-point is used for k-point sampling. The Fe_5Si_3 cluster consists of 128 atoms, placed in a cubic supercell with edge length of 30 Å to ensure that there is no interaction between neighboring clusters. The atomic positions for the clusters are full relaxed until the force acting on each atom is less than 0.1 eV/ Å. The convergence criterion of 10^{-5} eV has been used for electronic structure and density of states (DOS) calculations (see Fig. A1).

Appendix B. Extensions of the LSDA

It is sometimes claimed that density-functional theory (DFT) contains correlations and that approaches like the LSDA + U method account for correlations. This argumentation has three caveats. First, density-functional theory (DFT) provides an exact description of ground-state properties [33,64–66], but the density functional is generally unknown. The LSDA [10,59,67,68] is motivated by and adapted to itinerant electrons, while other density functionals bear little or no resemblance to the LSDA. Examples are the Runge-Zwicknagel functional for highly correlated electrons [62] and the density functional describing the crystal-field interaction of rare-earth 4f electrons [63].

Second, the determination of the Curie temperature involves excited states, which go beyond the scope of density-functional theory. Third, some correlation effects are only indirectly relevant to the Curie-temperature problem, because they do not address wave-function-specific features. In the LDA, the electron density is $n(\boldsymbol{r}) = \Sigma_i \phi_i^*(\boldsymbol{r})\phi_i(\boldsymbol{r})$, where the $\phi_i(\boldsymbol{r})$ are the eigenfunctions of

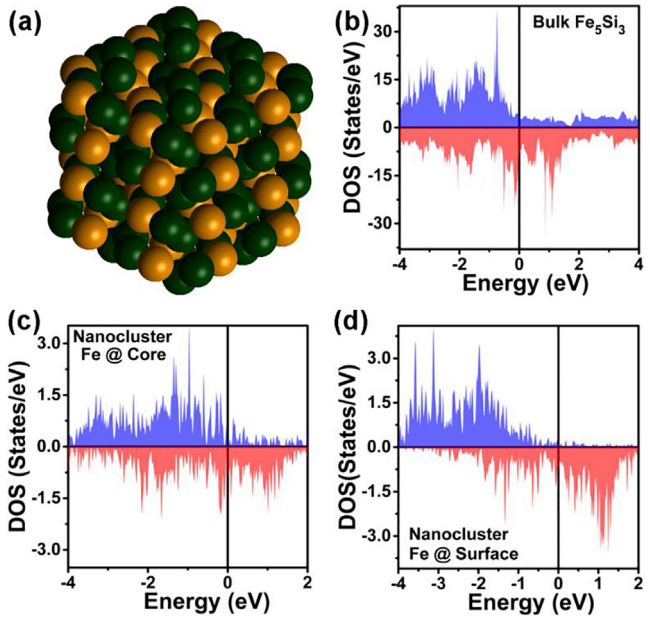

Fig. A1. Fe_5Si_3 nanoparticle densities of states (DOS) from DFT calculations: (a) structure, (b) bulk DOS, (c) nanoparticle DOS at the particle core and (d) DOS at the particle surface.

the Kohn-Sham (KS) equation [59]. These eigenfunctions are not physical wave functions but vehicles to construct the density $n(\mathbf{r})$. This point is made very clear in Kohn's Nobel Lecture [64], where he emphasized that in DFT "the electron density distribution $n(\mathbf{r})$, rather than the many-electron wave function, plays a central role". Density-functional approaches that depend exclusively on $n(\mathbf{r})$ but not separately on the eigenfunctions $\phi_i(\mathbf{r})$ are known as *orbital-free density-functional theory* (OF-DFT), but little is known about the corresponding density functionals, and existing functionals do not reproduce the kinetic energy very well [69-71]. The wave functions of many-electron systems, which are combinations of Slater determinants constructed from one-electron wave functions $\psi(\mathbf{r})$, $\psi'(\mathbf{r}')$, $\psi''(\mathbf{r}'')$, ..., $\psi_N(\mathbf{r}_N)$, cannot be reduced to KS eigenfunctions $\phi_i(\mathbf{r})$. Weakly correlated systems are an exception, because a Slater determinant created from the $\phi_i(\mathbf{r})$ can be used as zeroth-order eigenfunctions of many-electron perturbation theory.

The main point of the previous subsection, namely the reduction of the AFM energy due to many-electron correlations, is very general [3]. Uncorrelated pairs of ↑ and ↓ electrons can come very close to each other, which carries a penalty due to Coulomb repulsion. Correlation means that the electrons stay away from each other and thereby reduce their energy. Only ↑↓ pairs are affected by this reduction, because the Pauli principle forbids closely spaced ↑↑ electron pairs. For this reason, quantum-mechanical mean-field or selfconsistent-field (SCF) theories, such as LSDA, tend to overestimate the Curie temperature.

From a broader prospective, the main purpose of DFT is to describe the behavior of electrons in an external crystal-field potential $V(\mathbf{r})$ created by individual atoms, generally including thermal disorder. The total energy of the system is therefore a functional of $V(\mathbf{r})$ [72]. The relation between $n(\mathbf{r})$ and $V(\mathbf{r})$ is equivalent to the relation between the entropy S and the temperature T in statistical mechanics, and $n(\mathbf{r})$ and $V(\mathbf{r})$ are linked by a *Legendre transformation* similar to that linking S and T [63,73–75]. In this analogy, the density functional corresponds to the partition function $\mathcal{Z}$, which can be considered as the generating functional for thermodynamic properties. The knowledge of $\mathcal{Z}$, or of the free energy $F = -k_BT \ln \mathcal{Z}$, is necessary and sufficient to determine the equilibrium state at any temperature, which makes the calculation of $\mathcal{Z}$ the focus of statistical mechanics. Similarly, the density functional determines the ground-state behavior for arbitrary crystal potentials $V(\mathbf{r})$, but the real challenge is to calculate the analogue of the partition function, namely the density functional. This is not done in the LSDA, whose density is an intelligent and experimentally supported guess rather than the result of a calculation. The situation is similar to high-temperature analysis in statistical mechanics, where phenomenological guesses or series expansions yield approximate partition functions $\mathcal{Z}(T)$ that are limited to high temperatures, as LSDA is adapted to weakly correlated systems.

The LSDA + U method [76,77] modifies the KS one-electron potential by a potential that depends on the electron's orbital i, essentially [77]

$$V_i(\mathbf{r}) = V_{\mathrm{LSDA}}(\mathbf{r}) + U(1/2 - n_i) \tag{17}$$

where $U \sim \mathcal{U}$. This modification suppresses ↑↓ occupancies in highly correlated 3d and 4f orbitals and therefore partially accounts for correlations, especially with respect to on-site interactions [78]. In fact, it has been known for a long time that single Slater determinants using specifically adapted wave functions (unrestricted Hartree-Fock) include some, but not all, correlation contributions [10,79].

Eq. (17) optimizes the KS eigenfunctions but does not shake off the straightjacket of independent-electron theory. For example, it is known that large values of U lead to Mott localization [10,13,80,81], where the Coulomb repulsion completely suppresses the interatomic hopping of the electrons (metal-insulator transition), but in periodic crystals, the eigenfunctions belonging to Eq. (17) remain delocalized. As emphasized by Ashcroft and Mermin [3], such periodic eigenfunctions do not describe Mott localization but correspond to an extreme tight-binding approximation with small but metallic conductivity. This situation is very different from Anderson localization caused by aperiodic crystal potentials, for example at defects and surfaces. Anderson localization is well-described by independent-electron theory and means that

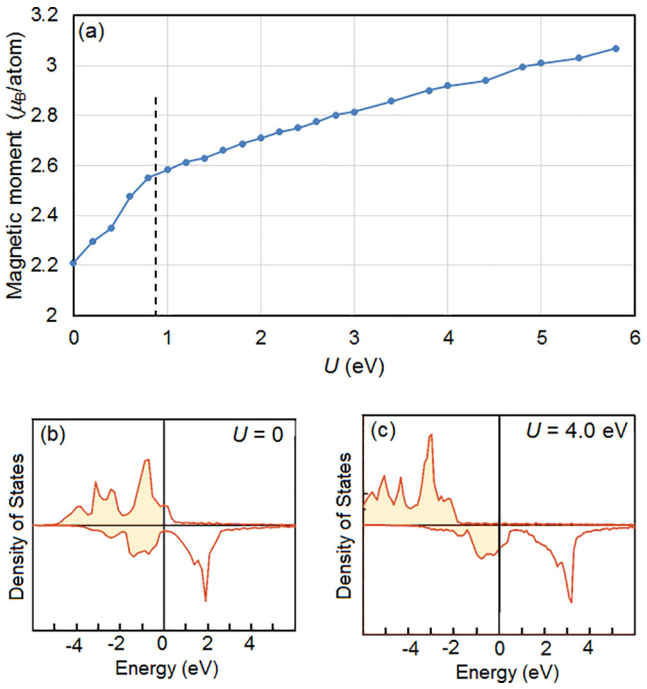

Fig. A2. LSDA + U for bcc Fe: (a) magnetic moment, (b) weak ferromagnetism and (c) strong ferromagnetism.

electrons may be "localized" in parts of a unit cell, which then repeats itself in the lattice, or truly localized due to broken periodicity [12].

A practical aspect of the LSDA + U method is that U is a well-defined first-principle quantity [77], not a fitting parameter in an approach where "plus U" is anecdotally interpreted as "plus you". Since $\mathcal{J} \sim m^2$, the choice of U has an indirect but substantial effect on T_c. Fig. A2 illustrates this point for the magnetic moment of bcc Fe, as calculated using the Vienna *ab initio* simulation package (VASP) [95] with U varying from zero to 6 eV and zero direct-exchange parameter (Fig. A2). The moment m per Fe atom (a) exhibits an increase from 2.21 μ_B to 3.07 μ_B, the experimental value being about 2.22 μ_B. Near $U = 0.9$ eV (dashed line in Fig. A2), the slope dm/dU changes from about 0.4 μ_B/eV to 0.1 μ_B/eV. This change is caused by an unphysical transition from weak ferromagnetism (holes in the minority 3d band) to strong ferromagnetism (b–c). Such a transition actually occurs in Fe_5Si_3, but it is due to nanostructuring (Section 5).

References

[1] W. Heisenberg, Zur Theorie des Ferromagnetismus, Z. Phys. 49 (1928) 619–636.
[2] S. Chikazumi, Physics of Magnetism, Wiley, New York, 1964.
[3] N.W. Ashcroft, N.D. Mermin, Solid State Physics, Saunders, Philadelphia, 1976.
[4] F. Bloch, Bemerkung zur Elektronentheorie des Ferromagnetismus und der elektrischen Leitfähigkeit, Z. Physik 57 (1929) 545–555.
[5] E.P. Wohlfarth, Very weak itinerant ferromagnets; application to $ZrZn_2$, J. Appl. Phys. 39 (1968) 1061–1066.
[6] K.K. Murata, S. Doniach, Theory of Magnetic Fluctuations in Itinerant Ferromagnets, Phys. Rev. Lett. 29 (1972) 285–288.
[7] P. Mohn, E.P. Wohlfarth, The Curie temperature of the ferromagnetic transition metals and their compounds, J. Phys. F 17 (1987) 2421–2430.
[8] T. Moriya, Spin Fluctuations in Itinerant Electron Magnetism, Springer, Berlin, 1985.
[9] R. Skomski, J.M.D. Coey, Permanent Magnetism, Institute of Physics, Bristol, 1999.
[10] P. Fulde, Electron Correlations in Molecules and Solids, Springer, Berlin, 1991.
[11] A.I. Liechtenstein, M.I. Katsnelson, V.P. Antropov, V.A. Gubanov, Local spin density functional approach to the theory of exchange interactions in ferromagnetic metals and alloys, J. Magn. Magn. Mater. 67 (1987) 65–74.
[12] E.N. Economou, Green's Functions in Quantum Physics, Springer, Berlin, 1979.
[13] N.F. Mott, Metal-Insulator Transitions, Taylor and Francis, London, 1974.
[14] R.M. Bozorth, Ferromagnetism, van Nostrand, Princeton, New Jersey, 1951.
[15] L. Liao, Y.-C. Lin, M. Bao, R. Cheng, J. Bai, Y. Liu, Y. Qu, K.L. Wang, Y. Huang, X. Duan, High-speed graphene transistors with a self-aligned nanowire gate, Nature 467 (2010) 305–308.
[16] P.C. Srivastava, J.K. Tripathi, Giant magnetoresistance (GMR) in swift heavy ion irradiated Fe films on c-silicon (Fe/c-Si), J. Phys. D Appl. Phys. 39 (2006) 1465–1471.
[17] Y. Jing, J.-M. Liu, W.-H. Ji, W. Wang, Sh.-H. He, X.-Z. Jiang, T. Wiedmann, Ch. Wang, J.-P. Wang, Biocompatible Fe – Si nanoparticles with adjustable self-regulation of temperature for medical applications, ACS Appl. Mater. Interfaces 7 (2015) 12649–12654.
[18] T. Shinjo, Y. Nakamura, N. Shikazono, Magnetic Study of Fe_3Si and Fe_5Si_3 by Mössbauer effect, J. Phys. Soc. Jap. 18 (1963) 797–801.
[19] H. Okamoto, Desk Handbook: Phase Diagrams for Binary Alloys, ASM International, Materials Park, OH, 2000, p. 374.
[20] S.A. Lyashchenko, Z.I. Popov, S.N. Varnakov, E.A. Popov, M.S. Molokeev, I.A. Yakovlev, A.A. Kuzubov, S.G. Ovchinnikov, T.S. Shamirzaev, A.V. Latyshev, A.A. Saranin, Analysis of optical and magnetooptical spectra of Fe_5Si_3 and Fe_3Si magnetic silicides using spectral magnetoellipsometry, J. Exp. Theor. Phys 120 (2015) 886–893.
[21] M.K. Kolel-Veetil, S.B. Qadri, M. Osofsky, R. Goswami, T.M. Keller, Carbon nanocapsule-mediated formation of ferromagnetic fe_5si_3 nanoparticles, J. Phys. Chem. C 113 (2009) 14663–14671.
[22] K. Seo, S. Lee, Y. Jo, M.-H. Jung, J. Kim, D.G. Churchill, B. Kim, Room Temperature Ferromagnetism in Single-Crystalline Fe_5Si_3 Nanowires, J. Phys. Chem. C 113 (2009) 6902–6905.
[23] B. Balasubramanian, P. Manchanda, R. Skomski, P. Mukherjee, B. Das, T.A. George, G.C. Hadjipanayis, D.J. Sellmyer, Unusual spin correlations in a nanomagnet, Appl. Phys. Lett. 106 (2015).
[24] P. Mohn, Magnetism in the Solid State, Springer, Berlin, 2003.
[25] R. Skomski, B. Balamurugan, P. Manchanda, M. Chipara, D.J. Sellmyer, Size dependence of nanoparticle magnetization, IEEE Trans. Magn. 53 (2017) 1–7.
[26] W. Jones, N.H. March, Theoretical Solid State Physics I, Wiley & Sons, London, 1973.
[27] R. Skomski, Simple Models of Magnetism, University Press, Oxford, 2008.
[28] A.J. Pindor, J. Staunton, G.M. Stocks, H. Winter, Disordered local moment state of magnetic transition metals: a self-consistent KKR CPA calculation, J. Phys. F: Met. Phys. 13 (1983) 979–990.
[29] J. Kübler, K.-H. Hock, J. Sticht, A.R. Williams, Density functional theory of non-collinear magnetism, Phys. F: Met. Phys. 18 (1988) 469–484.
[30] D. Hobbs, G. Kresse, J. Hafner, Fully unconstrained noncollinear magnetism within the projector augmented-wave method, Phys. Rev. B 62 (2000) 11556–11570.
[31] A. Avella, F. Manchini (Eds.), Strongly Correlated Systems: Numerical Methods, Springer, Berlin, 2013.
[32] G. Senatore, N.H. March, Recent progress in the field of electron correlation, Rev. Mod. Phys. 66 (1994) 445–479.
[33] A. Avella, F. Manchini (Eds.), Strongly Correlated Systems: Theoretical Methods, Springer, Berlin, 2012.
[34] W. Kohn, A. Yaniv, Locality principle in wave mechanics, Proc. Natl. Acad. Sci. USA 75 (11) (1978) 5270–5272.
[35] F. Cyrot-Lackmann, Sur le calcul de la cohésion et de la tension superficielle des métaux de transition par une méthode de liaisons fortes, J. Phys. Chem. Solids 1235–1243 (1968) 29.
[36] D.-Sh. Wang, R.-Q. Wu, A.J. Freeman, First-principles theory of surface magnetocrystalline anisotropy and the diatomic-pair model, Phys. Rev. B 47 (1993) 14932–14947.
[37] R. Skomski, A. Kashyap, A. Solanki, A. Enders, D.J. Sellmyer, Magnetic anisotropy in itinerant magnets, J. Appl. Phys. 107 (2010).
[38] J.S. Smart, Effective Field Theories of Magnetism, Saunders, Philadelphia, 1966.
[39] J.P. Perdew, K. Burke, M. Ernzerhof, Generalized gradient approximation made simple, Phys. Rev. Lett. 77 (1996) 3865–3868.
[40] F. Aryasetiawan, O. Gunnarsson, Electronic structure of NiO in the GW approximation, Phys. Rev. Lett. 74 (1995) 3221–3224.
[41] J.P. Perdew, A. Zunger, Self-interaction correction to density-functional approximations for many-electron systems, Phys. Rev. B 23 (1981) 5048–5079.
[42] W. Metzner, D. Vollhardt, Correlated lattice fermions in $d = \infty$ dimensions, Phys. Rev. Lett. 62 (1989) 324–327.
[43] M.J. Rozenberg, X.Y. Zhang, G. Kotliar, Mott-Hubbard transition in infinite dimensions, Phys. Rev. Lett. 69 (1992) 1236.
[44] M. Jarrell, Hubbard model in infinite dimensions: a quantum Monte Carlo study, Phys. Rev. Lett. 69 (1992) 168–171.
[45] U. Schollwöck, The density-matrix renormalization group, Rev. Mod. Phys. 77 (2005) 259–315.
[46] T.D. Lee, C.N. Yang, Statistical theory of state and phase equations: lattice gas and Ising model, Phys. Rev. 87 (1952) 410–419.
[47] Bh. Das, B. Balamurugan, P. Manchanda, P. Mukherjee, R. Skomski, G.C. Hadjipanayis, D.J. Sellmyer, Mn_5Si_3 nanoparticles: synthesis and size-induced ferromagnetism, Nano Lett. 16 (2016) 1132–1137.
[48] L. Néel, Antiferromagnetism and ferrmagnetism, Proc. Phys. Soc. A 65 869–885.
[49] J.S. Smart, The Néel Theory of ferrimagnetism, Am. J. Phys. 23 (1955) 356–370.
[50] R. Skomski, D.J. Sellmyer, Curie Temperature of Multiphase Nanostructures, J. Appl. Phys. 87 (2000) 4756–4758.
[51] W. Kohn, N. Rostoker, Solution of the Schrödinger equation in periodic lattices with an application to metallic lithium, Phys. Rev. 94 (5) (1954) 1111–1120.
[52] T. Huhne, C. Zecha, H. Ebert, P.H. Dederichs, R. Zeller, Full-potential spin-polarized relativistic Korringa-Kohn-Rostoker method implemented and applied to bcc Fe, fcc Co, and fcc Ni, Phys. Rev. B 58 (1998) 10236–19247.
[53] H. Ebert, A spin polarized relativistic Korringa-Kohn-Rostoker (SPR-KKR) code for calculating solid state properties, http://olymp.cup.uni-muenchen.de/ak/ebert/SPRKKR, LMU Munich, 2012.
[54] R. Skomski, C. Waldfried, P.A. Dowben, The influence of the surface on the spontaneous magnetization of Gd thin films, J. Phys.: Condens. Matter 10 (1998) 5833–5838.
[55] K.G. Wilson, The renormalization group and critical phenomena, Rev. Mod. Phys. 55 (1983) 583–600.
[56] J.M. Yeomans, Statistical Mechanics of Phase Transitions, University Press, Oxford, 1992.
[57] D. Böttcher, A. Ernst, J. Henk, Temperature-dependent Heisenberg exchange coupling constants from linking electronic-structure calculations and Monte Carlo simulations, J. Magn. Magn. Mater. 324 (2012) 610–615.
[58] P. Hohenberg, W. Kohn, Inhomogeneous Electron Gas, Phys. Rev. 136 (1964) B864–B871.
[59] W. Kohn, L.J. Sham, Self-consistent equations including exchange and correlation effects, Phys. Rev. 140 (1965) A1133–A1138.
[60] L.J. Sham, W. Kohn, One-particle properties of an inhomogeneous interacting electron gas, Phys. Rev. 145 (1966) 561–567.
[61] S.G. Ovchinnikov, S.N. Varnakov, S.A. Lyashchenko, I.A. Tarasov, I.A. Yakovlev, E.A. Popov, S.M. Zharkov, D.A. Velikanov, A.S. Tarasov, V.S. Zhandun, N.G. Zamkova, Iron silicide-based ferromagnetic metal/semiconductor nanostructures, Phys. Sol. State 58 (2016) 2277–2281.
[62] E. Runge, G. Zwicknagl, Electronic structure calculations and strong correlations: a model study, Ann. Physik 5 (1996) 333–354.
[63] R. Skomski, P. Manchanda, A. Kashyap, Correlations in rare-earth transition-metal permanent magnets, J. Appl. Phys. 117 (2015).
[64] W. Kohn, Nobel lecture: electronic structure of matter—wave functions and density functionals, Rev. Mod. Phys. 71 (1999) 1253–1266.
[65] R.O. Jones, O. Gunnarson, The density functional formalism, its applications and prospects, Rev. Mod. Phys. 61 (1989) 689–746.

[66] M.S.S. Brooks, Calculated ground state properties of light actinide metals and their compounds, Physica B 130 (1985) 6–12.
[67] U. von Barth, L. Hedin, A local exchange-correlation potential for the spin polarized case, J. Phys. C 5 (1972) 1629–1642.
[68] O. Gunnarsson, B.I. Lundqvist, Exchange and Correlation in atoms, molecules, and solids by the spin-density-functional formalism, Phys. Rev. B 13 (1976) 4274.
[69] L.-W. Wang, M.P. Teter, Kinetic-energy functional of the electron density, Phys. Rev. B 45 (1992) 13196–13220.
[70] D.R. Murphy, Sixth-order term of the gradient expansion of the kinetic-energy density functional, Phys. Rev. A 24 (1981) 1682–1688.
[71] S. Kümmel, L. Kronik, Orbital-dependent density functionals: Theory and applications, Rev. Mod. Phys. 80 (2008) 3–60.
[72] The difference between scalar functions, vector functions, and functionals is mathematical rather than physical, epitomized by the respective products a b, a·b = Σi ai bi, and ∫ a(r) b(r) dr.
[73] R. Fukuda, T. Kotani, Y. Suzuki, S. Yokojima, Density functional theory through legendre transformation, Prog. Theor. Phys. 92 (1994) 833–862.
[74] E.H. Lieb, Density functionals for coulomb systems, Int. J. Quantum Chem. 24 (1983) 243–277.
[75] N. Argaman, G. Makov, Density Functional Theory: An Introduction, Am. J. Phys. 68 (2000) 69–79.
[76] V.I. Anisimov, J. Zaanen, O.K. Andersen, Band theory and Mott insulators: hubbard U instead of Stoner I, Phys. Rev. B 44 (1991) 943–954.
[77] V.I. Anisimov, F. Aryasetiawan, A.I. Lichtenstein, First-principles calculations of the electronic structure and spectra of strongly correlated systems: the LDA+ U method, J. Phys.: Condens. Matter 9 (1997) 767–808.
[78] J. Zaanen, G.A. Sawatzky, J.W. Allen, Band gaps and electronic structure of transition-metal compounds, Phys. Rev. Lett. 55 (1985) 418–421.
[79] C.A. Coulson, I. Fischer, Notes on the molecular orbital treatment of the hydrogen molecule, Philos. Mag. 40 (1949) 386–393.
[80] J. Hubbard, Electron correlations in narrow energy bands, Proc. R. Soc. London Ser. A 276 (1963) 238–257.
[81] W.F. Brinkman, T.M. Rice, Application of Gutzwiller's variational method to the metal-insulator transition, Phys. Rev. B 2 (1970) 4302–4304.
[82] G. Kresse, J. Hafner, Ab initio molecular dynamics for open-shell transition metals, Phys. Rev. B 48 (1993) 13115–13118.
[83] M.A. Nielsen, I.L. Chuang, Quantum Computation and Quantum Information, University Press, Cambridge, 2000.
[84] G. Burkard, D. Loss, D.P. DiVincenzo, Coupled Quantum Dots as Quantum Gates, Phys. Rev. B 59 (1999) 2070–2078.
[85] R. Skomski, A.Y. Istomin, A.F. Starace, D.J. Sellmyer, Quantum entanglement of anisotropic magnetic nanodots, Phys. Rev. A 70 (2004).
[86] V.V. França, K. Capelle, Entanglement in spatially inhomogeneous many-fermion systems, Phys. Rev. Lett. 100 (2008).
[87] J. Eisert, M. Cramer, M.B. Plenio, Colloquium: area laws for the entanglement entropy, Rev. Mod. Phys. 82 (2010) 277–306.
[88] A.J. Schofield, Non-Fermi liquids, Contemporary Phys. 40 (1999) 95–115.
[89] J.M. Luttinger, An Exactly Soluble Model of a Many-Fermion System, J. Math. Phys. 4 (1963) 1154–1162.
[90] M. Karbach, G. Müller, Introduction to the Bethe ansatz I, Comput. Phys. 11 (1997) 36–44.
[91] M. Karbach, K. Hu, G. Müller, Introduction to the Bethe ansatz II, Comput. Phys. 12 (1998) 565–573.
[92] D. Bitko, T.F. Rosenbaum, G. Aeppli, Quantum critical behavior for a model magnet, Phys. Rev. Lett. 77 (1996) 940–943.
[93] X.-G. Wen, Quantum-Field Theory of Many-Body Systems, University Press, Oxford, 2004.
[94] G. Kresse, D. Joubert, From ultrasoft pseudopotentials to the projector augmented-wave method, Phys. Rev. B 59 (1999) 1758–1775.
[95] G. Kresse, J. Hafner, *Ab initio* molecular dynamics for liquid metals, Phys. Rev. B 47 (1993) 558–561.
[96] G. Kresse, J. Furthmüller, Efficiency of ab-initio total energy calculations for metals and semiconductors using a plane-wave basis set, Comp. Mater. Sci. 6 (1996) 15–50.
[97] H.J. Monkhorst, J.D. Pack, Special points for Brillonin-zone integrations, Phys. Rev. B 13 (1976) 5188–5192.